of a real-space approach with the possibility of working directly with the measured data as typical in reciprocal-space methods.

3.6.3. Examples of WPPM analysis

To illustrate the power of the WPPM approach, a few examples are provided based both on simulated and on real data. The analyses were performed using the *PM2K* software (Leoni *et al.*, 2006). Similar results are obtained using the WPPM implementation in the commercial program *TOPAS*.

3.6.3.1. *Nanocrystalline ceria*

The first example concerns a nanocrystalline ceria powder obtained by the calcination of a cerium isopropoxide gel (Leoni, Di Maggio *et al.*, 2004; Leoni & Scardi, 2004; Scardi *et al.*, 2004). A large amount of XRD and transmisson electron microscopy (TEM) data have been collected on the same system (and specimen), starting from the xerogel and following calcination (Scardi *et al.*, 2010). Fig. 3.6.1(*a*) shows the X-ray powder diffraction pattern of the gel calcined for 1 h at 673 K measured with Cu radiation (40 kV, 45 mA) on a Rigaku PMG/VH diffractometer.

The data were collected over the 2θ range 18–154° (with a step of 0.05°) with a counting time of 60 s per step: a wide angular range and a high signal-to-noise ratio (SNR) are prerequisites for a proper line-profile analysis. The large span in reciprocal space is important for the complete characterization of any anisotropy in the broadening (a large set of independent directions in reciprocal space needs to be sampled), whereas the high SNR guarantees the collection of data at peak tails where the differences between similar microstructure models manifest themselves. The log scale employed in Fig. 3.6.1(*a*) highlights the low level of noise present in the pattern.

The diffractometer had 0.5° divergence and 2° Soller slits mounted on the primary arm and 0.15 mm antiscatter, 0.5° receiving and 2° Soller slits and a curved graphite analyzer crystal mounted on the secondary arm. This setup provided a narrow and symmetrical instrumental profile that could be described by a pseudo-Voigt curve and was thus ideal for line-profile analysis studies. The Caglioti *et al.* (1958) parameterization of the instrumental profile [*cf.* equations (3.6.18) and (3.6.19)] performed on the profiles of the NIST SRM 660a standard (LaB_6) is shown in Fig. 3.6.2.

Analysis of the pattern using traditional methods (see Scardi *et al.*, 2004) required 59 parameters, 53 of which were actually refined:

(i) one unit-cell parameter (a_0),
(ii) six (fixed) parameters defining the instrumental contribution [five parameters for the Caglioti parameterization (U, V, W, a and b) and one for the $K\alpha_2$ intensity ratio],
(iii) three parameters for the background,
(iv) one parameter for the specimen displacement,
(v) 48 parameters for the peaks (intensity, FWHM and shape for 16 peaks).

An analysis using traditional analysis methods resulted in an 'average domain size' of 3.65 (10) nm using the (modified) Warren–Averbach method and in the range from 4.95 (10) to 5.3 (1) nm using a (modified) Williamson–Hall approach. A discussion of the meaning and accuracy of the results can be found in Scardi *et al.* (2004).

The WPPM result, shown in Fig. 3.6.1(*b*), matches the experiment quite well: this is remarkable considering that the whole pattern (1800 data points) is modelled using just 32 parameters (26 free parameters):

(i) one unit-cell parameter (a_0),
(ii) six (fixed) parameters defining the instrumental contribution [five parameters for the Caglioti parameterization (U, V, W, a and b) and one for the $K\alpha_2$ intensity ratio],

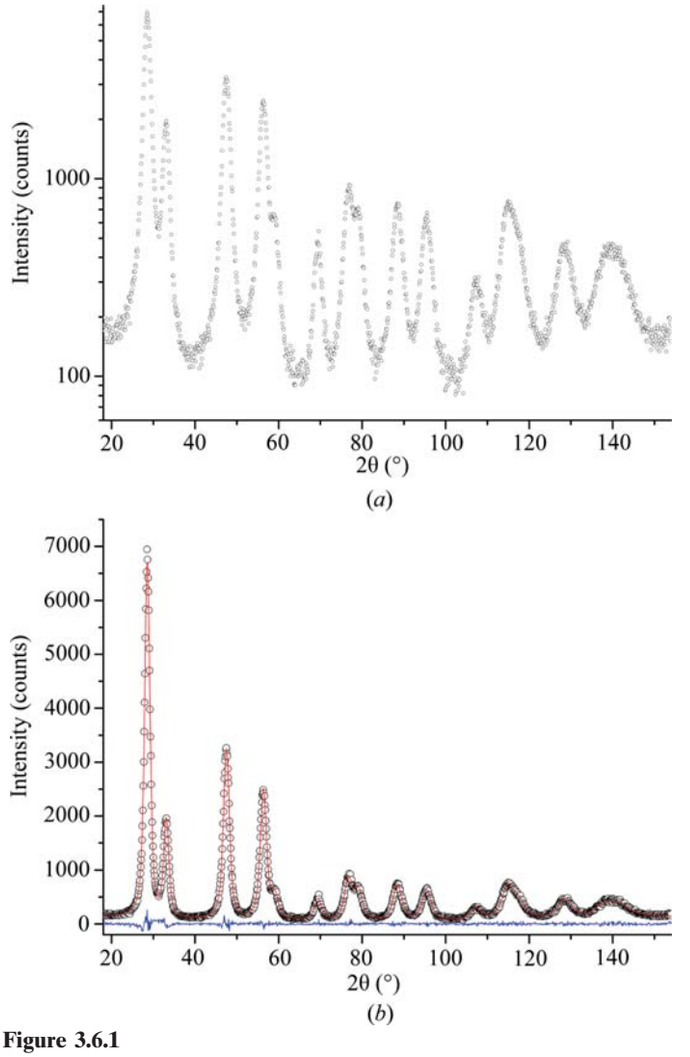

Figure 3.6.1
X-ray powder diffraction pattern of nanocrystalline ceria calcined at 673 K. In (*a*) the pattern is shown on a log scale to highlight the weak features in the data. In (*b*) the results of WPPM are shown: raw data (dots), model (line) and difference (lower line).

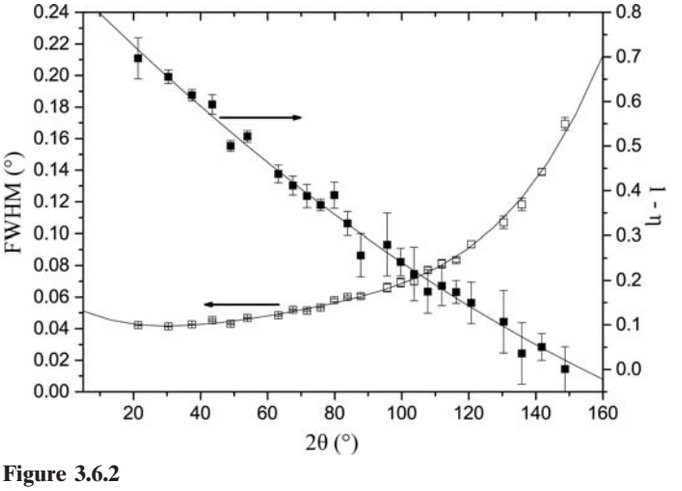

Figure 3.6.2
Parameterization of the instrumental resolution function using a pseudo-Voigt and the relationship of Caglioti *et al.* (1958).

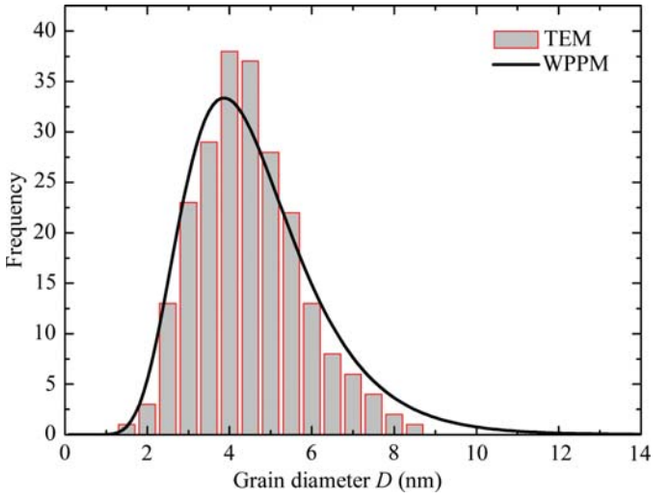

Figure 3.6.3
Size distribution of the ceria powder: WPPM (line) and TEM (histogram).

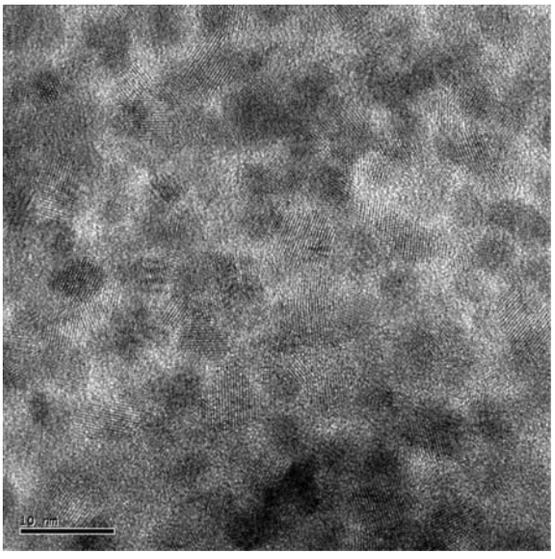

Figure 3.6.4
TEM micrograph of the calcined ceria powder. The scale bar represents 10 nm.

(iii) two parameters for the log-normal size distribution (μ and σ),
(iv) three parameters for the dislocation contributions (ρ, R_e and the mixing parameter f_e),
(v) three parameters for the background,
(vi) one parameter for the specimen displacement,
(vii) 16 parameters for the intensity of the peaks.

It is therefore possible to obtain more complete results with a number of parameters that is dramatically lower than that needed for the traditional analysis: the shapes of the peaks are interlinked *via* the microstructure models. It is suggested that the parameters are initialized with values providing a minimal but measurable effect (*i.e.*, for instance, $\mu = 2$, $\sigma = 0.4$, $\rho = 10^{15}$ m^{-2}, $f_e = 0.5$) to favour a rapid convergence.

By way of a check, Fig. 3.6.3 shows the good agreement between the size distribution obtained by WPPM and that obtained on the same specimen from the analysis of a large set of TEM micrographs (800 grains surveyed; Fig. 3.6.4). The data were collected on a 300 kV JEOL 3010 microscope (0.17 nm point-to-point resolution) equipped with a Gatan slow-scan 974 CCD camera (Leoni, Di Maggio *et al.*, 2004). Even if the particles are well separated, the analysis is quite tedious and prone to bias from the operator. The large and small particles are in fact easily missed, and overlapping particles are hard to separate and are usually not considered. Moreover, only the cross section is measured, as the transverse direction is difficult to access.

The statistical validity of the WPPM result is quite clear: a few million grains are probed by the X-rays *versus* the few hundred actually considered in microscopy. The WPPM result allows not only the mean (first moment) and variance to be obtained from the refined size distribution, but also the recovery of the most probable values for the traditional results (we know the shape and we can weight the column-length distribution by the surface or by the volume). In this case the numerical mean is ~4.3 nm: we can immediately understand the risk of placing faith in the results of a traditional analysis. The agreement between TEM and XRD is in any case excellent. The residual differences may be due both to the issues related to sizing under the microscope and to the simplified treatment employed in the WPPM (perfectly spherical domains, monodisperse shape, absence of surface relaxation *etc.*). A more complex model (accounting, for example, for surface relaxation effects) can be considered (see Scardi & Leoni, 2002; Leoni & Scardi, 2004), but the effects on the distribution are minimal.

The possibility of extracting information on the type of defects (*e.g.* dislocations, faults and APDBs) and on their amount is definitely a major advantage of WPPM over traditional methods and over TEM. For the determination of the dislocation density, the average contrast factor is needed; the actual expressions can be readily obtained from the single-crystal elastic constants (c_{11} = 403, c_{12} = 105 and c_{44} = 60 GPa; Nakajima *et al.*, 1994) as

$$\overline{C}_{\mathrm{CeO_2},e} = 0.122945 + 0.358092\frac{h^2k^2 + k^2l^2 + h^2l^2}{(h^2 + k^2 + l^2)^2}, \qquad (3.6.54)$$

$$\overline{C}_{\mathrm{CeO_2},s} = 0.105762 + 0.207999\frac{h^2k^2 + k^2l^2 + h^2l^2}{(h^2 + k^2 + l^2)^2} \qquad (3.6.55)$$

for edge and screw dislocations, respectively.

A dislocation density of 1.4×10^{16} m^{-2} was obtained for the specimen analysed here. This dislocation density immediately appears to be quite high when compared with the number of dislocations that can be identified in high-resolution TEM micrographs, as it corresponds to approximately one dislocation every couple of grains (Leoni & Scardi, 2004). However, the dislocations visible in the micrographs are just a small fraction of the total: if a dislocation is not properly aligned with the zone axis, it is in fact invisible (its presence can only be inferred from the effects of the distortion field). It is true that a sufficiently large number of dislocations must be present in order to give appreciable effects on the diffraction pattern, and TEM is still the better technique if the density of dislocations is below, for example, 10^{14} m^{-2}.

3.6.3.2. *Copper oxide*

The true power of WPPM, and of diffraction in general, can be appreciated in multi-phase systems. The unequivocal assignment of a structure to each grain is definitely impossible using TEM, unless each grain is individually sampled and carefully analysed. It is therefore quite hard to identify the phases present in the specimen and to characterize their microstructure independently from a micrograph alone. Conversely, information on the various phases is well separated in a diffraction pattern. The various (known) phases in a specimen can easily be identified (for